
Article:
Cookson, NJ orcid.org/0000-0002-6048-4604, Fowler, JM orcid.org/0000-0001-8142-9084, Martin, DP orcid.org/0000-0001-8502-7795 et al. (6 more authors) (2018) Metallo-cryptophane cages from cis-linked and trans-linked strategies. Supramolecular Chemistry, 30 (4). pp. 255-266. ISSN 1061-0278

https://doi.org/10.1080/10610278.2017.1355055

Metallo-cryptophane cages from *cis*-linked and *trans*-linked strategies

Nikki J. Cookson,[a] Jonathan M. Fowler,[a] David P. Martin,[a] Julie Fisher,[a,c] James J. Henkelis,[a] Tanya K. Ronson,[a,b] Flora L. Thorp-Greenwood,[a] Charlotte E. Willans,[a] and Michaele J. Hardie.[a*]

[a] *School of Chemistry, University of Leeds, Leeds LS2 9JT, UK.* *m.j.hardie@leeds.ac.uk*

[b] *current address: Department of Chemistry, University of Cambridge, Cambridge CB2 1EW*

[c] *deceased 5th August 2015*

Metallo-cryptophane M_3L_2 cages from *cis*-linked and *trans*-linked strategies.

Trigonal bipyramidal metallo-cage species $[Pd_3(dppp)_3(L)_2]\cdot 6OTf$ (where dppp = bis(diphenylphosphino)propane, OTf = triflate and L is *tris*(iso-nicotinoyl)cyclotriguaiacylene (L1) or *tris*(fluoro-iso-nicotinoyl)cyclotriguaiacylene (FL1)) have been characterised in solution to existpredominantly as the *anti*-isomers. The crystal structure of $[Pd_3(dppp)_3(FL1)_2]\cdot 6OTf$, however, was found to be the achiral *syn*-isomer. The complex $[Pd_3Cl_3(L2)_2]$ (where L2 = *tris*(methylbenzimidazolyl)cyclotriguaiacylene) is a *trans*-linked M_3L_2 cage, observed by mass spectrometry and in the solid state as the *anti*-isomer. Ligand L2 also forms a 1:1 co-crystal with cyclotriguaiacylene.

Keywords: cyclotriveratrylene; metallo-cage; co-crystal; metallo-supramolecular chemistry

Introduction

Cryptophanes are capsule-like organic cage species composed of two cyclotriguaiacylene or related fragments linked together through three covalent spacers.[1] They have a rich history as host cage species, and are known to bind gases such as Xe[2] and small hydrocarbons.[3] Cyclotriguaiacylene (CTG, Figure 1) is a member of the cyclotriveratrylene family of host molecules which feature a tribenzo[a,d,g]cyclononene scaffold with a bowl conformation. CTG is chiral with *M* and *P* isomers, hence crytophanes may form as achiral *syn*-isomers, or as chiral *anti*-isomers (Figure 1). Metallo-cryptophanes, or metallo-organic cryptophanes, are analogous metallo-cage species of M_3L_2 composition where L is a CTG-analogue decorated with transition metal-binding groups. They are one of the smallest metallo-cages that can be assembled from CTG-type ligands.[4] The first metallo-cryptophanes were reported by Yamaguchi and Shinkai, and their design linked 4-pyridyl-decorated

L-ligands in a *cis*-fashion using *cis*-protected square planar [Pd(P^P)] fragments, where P^P = bis(diphenylphosphino)ethane (dppe) or bis(diphenylphosphino)propane (dppp) (Figure 1).[5] Different P^P ligands result in different solution behaviour; for $[(Pd_3(dppe)_3(L)_2]^{6+}$ a 2.5:1 *syn*:*anti* equilibrium mixture results, but where P^P = dppp the initially formed *anti*-isomer disappears slowly until the *syn*-isomer predominates in solution. Chambron and co-workers have recently reported a series of $[M_3(dppp)_3L_2]^{6+}$ metallo-cryptophanes, where M = Pd(II) or Pt(II) and L is a nitrile-decorated CTG, or related, ligand (Figure 1b).[6] Here, the *anti*-isomers dominate in solution and the solid state, although small amounts of *syn*-isomer were observed for Pt(II) cages. The $[(Pd_3(dppe)_3(L)_2]^{6+}$ species where R = H (Figure 1b) converts from *anti*- to predominantly *syn*-isomer when cooled in CD_2Cl_2,. Research from our laboratories have employed different metal-chelate motifs to form metallo-cryptophanes with *cis*-arrangement of coordination groups. These are $[Pd_3(bis\text{-}NHC)_3L_2]$ cages, where bis-NHC is a naphthyl-appended bis-N-heterocyclic carbene ligand (Figure 1c),[7] and luminescent $[\{Ir(ppy)_2\}_3L_2]$ cages, where ppy is 2-phenylpyridine (Figure 1d).[8] The former crystallises as achiral *syn*-isomers, while the latter forms as *anti*-isomers.

M_3L_2 metallo-cryptophanes have also been reported without protecting auxillary chelating ligands from *trans* coordination of L-ligands at the metal centres, Figure 1e and 1f. In these examples, linear metal coordination occurred at Ag(I) or Cu(II) cations with 3-pyridyl or pyrimidine ligand donor groups appended to CTG.[9] These *trans*-linked cages form as the *anti*-isomers in the solid state, and the $[Ag_3L_2]^{3+}$ metallo-cryptophane (Figure 1e) actually forms as a [2]catenane of two interlocked cages. *Syn*-$\{(M_3L_2)_2\}$ cage catenane metallo-cryptophanes similarly form with bipyridine-appended CTG-ligands (Figure 1g).[10] M_3L_2 species related to metallo-cryptophanes can also be formed from achiral tripodal carboxylate-decorated cavitand ligands.[11] Capsule-

like metallo-cages have also been reported using other types of functionalised bowl-shaped host molecules, most commonly calix[4]arenes and resorcinarenes, and including examples of *cis*-linked [12] and *trans*-linked [13] and chelate-linked [14] capsules.

We report herein further investigations into both the *cis*-linked and *trans*-linked strategy to metallo-cryptophanes employing the classes of tripodal L-ligands developed in our laboratories. Such ligands appended with 4-pyridyl groups[5,7] (or linear nitrile as above[6]) suit the formation of a *cis*-linked metallo-cryptophane cage, and here we utilise two ligands appended with iso-nicotinyl groups: *tris*(iso-nicotinoyl)cyclotriguaiacylene L1, and *tris*(fluoro-iso-nicotinoyl)cyclotriguaiacylene (FL1), Scheme 1. CTG-ligands with iso-nicotinoyl ligand groups have been particularly successful ligands for metallo-supramolecular chemistry, forming M_3L_2 metallo-cryptophanes,[7] larger M_6L_8 cages,[15] alongside coordination polymers [16] and a M_6L_6 metallacycle with a unique infinite Borromean entanglement.[17] While previous reports of the *trans*-linked approach used 3-pyridyl donors,[9] here we investigate a 5-membered imidazole ring as the donor group with the novel ligand *tris*(methylbenzimidazolyl)cyclotriguaiacylene (L2, Scheme 1).

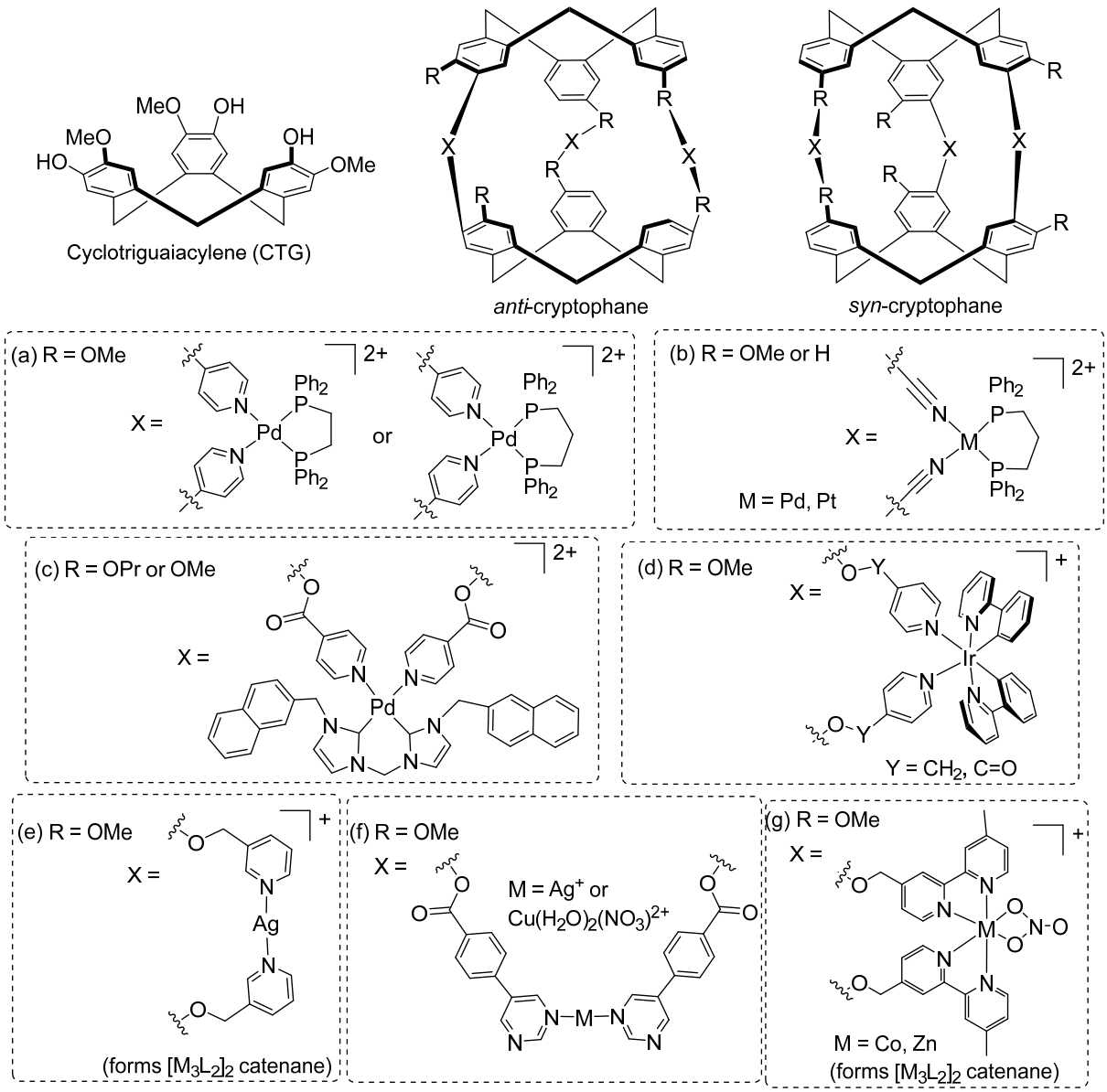

Figure 1: Cyclotriguaiacylene with general form of syn- and anti-cryptophanes and motifs used to form metallo-cryptophanes with (a)-(d) cis-coordination of CTG-type ligands at metal; (e)-(f) trans coordination at the metal; (g) from chelating ligand.[5-10]

Results and Discussion

Ligand synthesis and structures

The tripodal cyclotriguaiacylene ligands (±)-2,7,12-trimethoxy-3,8,13-*tris*(3-fluoro-4-pyridylcarboxy)-10,15-dihydro-5*H*-tribenzo[a,d,g]cyclononene (*tris*(fluoro-iso-nicotinoyl)cyclotriguaiacylene, FL1) and (±)-2,7,12-trimethoxy-3,8,13-*tris*(methylbenzimidazol-1-yl)-10,15-dihydro-5*H*-tribenzo[a,d,g]cyclononene (*tris*(methylbenzimidazolyl)cyclotriguaiacylene, L2) were synthesised as racemic mixtures from cyclotriguaiacylene according to Scheme 1. For FL1, the acid chloride of 3-fluoro-4-pyridine carboxylic acid was generated *in situ* then reacted with CTG in a basic environment to give (±)-FL1. Yields are maximised by addition of a second batch of the acid chloride reactant after an initial 2 days reaction time. Both ligands gave ^{1}H NMR spectra characteristic of bowl-conformation tripodal CTG derivatives with retention of high symmetry, and the diastereotopic *exo* and *endo* CH_2 protons giving doublets at 4.90 and 3.71 ppm for FL1, and 4.69 and 3.47 ppm for L2. The ^{19}F NMR spectrum of FL1 is the expected doublet of doublets which collapses to a singlet at -125.61 ppm in d_6-DMSO on broadband decoupling. The anticipated molecular ion peaks were observed by electrospray mass spectrometry.

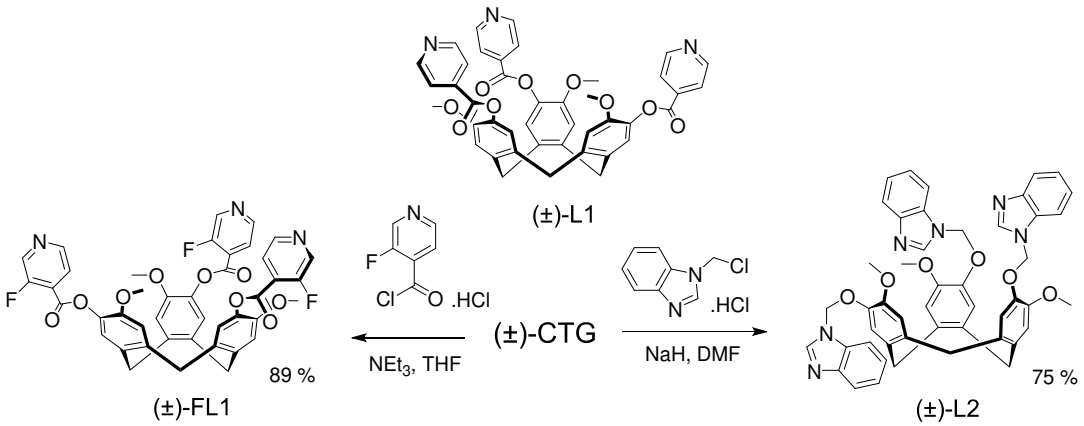

Scheme 1: Ligands used in this study with synthetic routes to FL1 and L2.

Single crystals of L2 suitable for X-ray analysis were obtained by slow evaporation of an acetone solution. L2 crystallises in a triclinic cell and the structure was solved in space group *P*-1. There is one complete molecule of L2 in the asymmetric unit. All three methylbenzimidazolyl arms of L2 have different orientations, and are folded back towards the molecular cavity of L2 effectively blocking any access for potential guests in this conformation, Figure 2. The C_{arene}-O-CH_2-N_{imid} torsion angles are 70.0, 85.1 and 63.6 °. There is a weak intramolecular C-H···N interaction between two benzimidazolyl at C···N separation 3.51 Å. In the crystal lattice, primitive layers of L2 ligands form in the *ab* plane and enantiomeric layers with inverted orientations stack together in the *c* direction, (supplementary information (SI) Fig. S39).

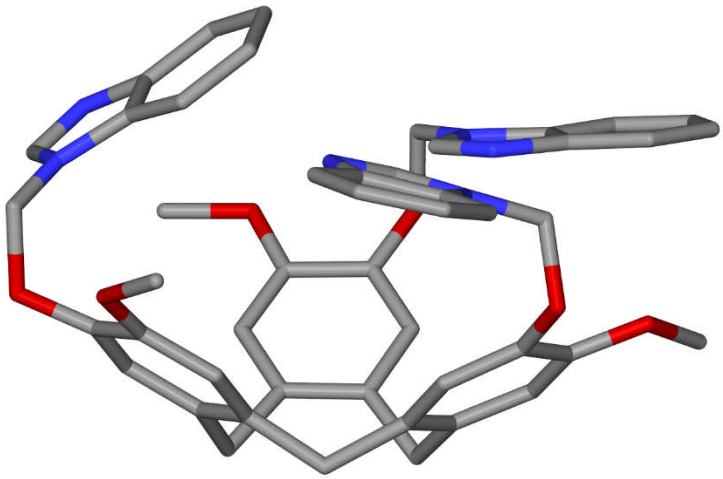

Figure 2. X-ray structure of L2 showing asymmetric unit.

Interestingly, L2 forms a co-crystal with its precursor CTG. This was initially obtained in low yield from the slow evaporation of an acetone solution of L2 containing some CTG contaminant, but the co-crystal can also be formed in bulk from a 1:1 mixture of L2 and CTG. The structure of complex (L2)·(CTG) was determined by single crystal X-ray diffraction using a synchrotron source. It crystallises in the non-centrosymmetric trigonal space group *Pc*31. The asymmetric unit comprises one third

of each component, with each molecular component having crystallographic 3-fold symmetry. Unlike in the structure of L2 itself, the methylbenzimidazolyl arms of L2 are oriented away from the cavitand bowl. Each molecule of L2 forms hydrogen bonding associations with three equivalent CTG molecules through OH···N hydrogen bonds (at O···N distance 2.79 Å). Similarly, each CTG hydrogen bonds to three equivalent L2 molecules to form a 2D network of 6^3 topology, Figure 3a. The CTG and L2 molecules within the network have opposite orientations of their molecular bowls and each network is homochiral. Networks pack together in the crystal lattice such that the chirality of the network alternates along *c*, and there is homoleptic and racemic bowl-in-bowl stacking of host molecules - that is, 1-D stacks of L2 molecules of alternating enantiomer form as do 1-D stacks of enantiomers of CTG, Figure 3b. Bowl-in-bowl stacking is a well-known motif for cyclotriveratrylene[18] though examples of its occurrence for CTG-analogues are rarer. It does not involve π-π stacking interactions between the host core and can occur in a racemic fashion as here,[15c,19] or involve formation of homochiral 1-D arrays.[15c,20]

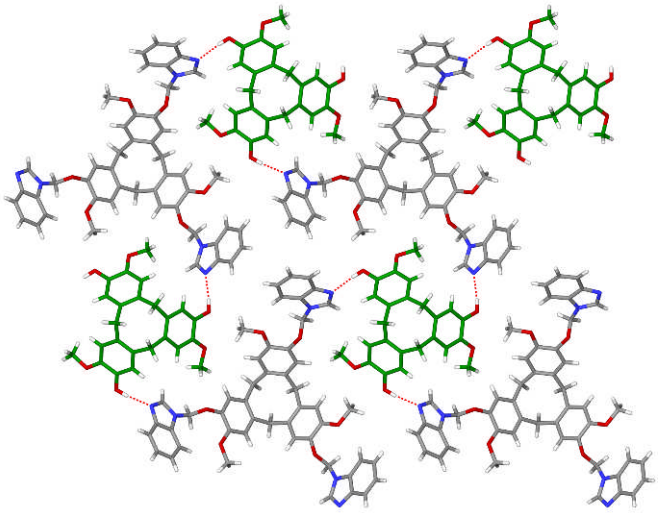

(a)

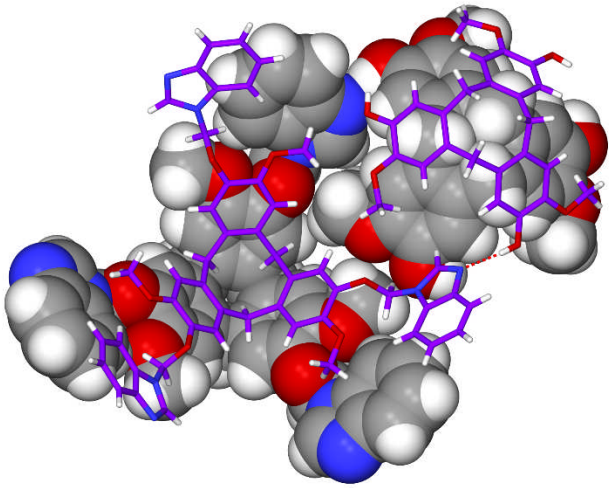

(b)

Figure 3. From the X-ray structure of (L2)·(CTG). (a) Section of a hydrogen bonded 2D network with CTG in green; (b) Stacking between networks highlighting homoleptic bowl-in-bowl stacking of enantiomers with molecules belonging to one hydrogen bonded layer in space-filling.

Cis-linked M_3L_2 cages with L1 or FL1

Use of chelating ligands to control the available coordination sites on the metal is a common strategy for metallo-cage assembly, most typically to ensure a *cis* stereochemistry of available sites. Alongside the bis-phosphines shown in Figure 1, the most commonly used chelating ligands are ethylenediamine (en) or derivatives.[21,22] Our prior attempts to form M_3L_2 metallo-cryptophane assemblies, where L = *tris*(isonicotinoyl)-*tris*(propyl)-cyclotricatechylene (R = OPr in Figure 1c), using [Pd(en)] as *cis*-protected metal fragments were unsuccessful.[7] While a metallo-cryptophane initially formed, it was metastable and equilibration resulted in displacement of the chelate ligands and formation of a $[Pd_6L_8]^{12+}$ cage. A similar $M_3(en)_3L_2$ to M_6L_8 rearrangement has also been reported by Chand for a different class of tripodal L ligand.[22] Attempts here to form $[Pd_3(en)_3(L)_2]^{6+}$ species, where L = L1 or FL1, in a variety of solvents were also unsuccessful. The ^{1}H NMR spectra obtained

were a superposition of the spectra of the L and $Pd(en)(NO_3)_2$ starting materials (SI Figs. S11-S13), and a metastable M_3L_2 species was not observed.

Instead we investigated bis-(diphenylphosphino)propane (dppp) as the *cis*-protecting ligand analogous to previous examples.[5,6] The square planar complex $[Pd(dppp)(OTf)_2]$ was employed as a *cis*-protected metallo-tecton for the assembly of a metallo-cryptophane with the 4-pyridyl-decorated hosts L1 and FL1 according to Scheme 2. Formation of the $[Pd_3(dppp)_3(L)_2]^{6+}$ metallo-cryptophane cages, where L = L1 or FL1, was studied by NMR spectroscopy.

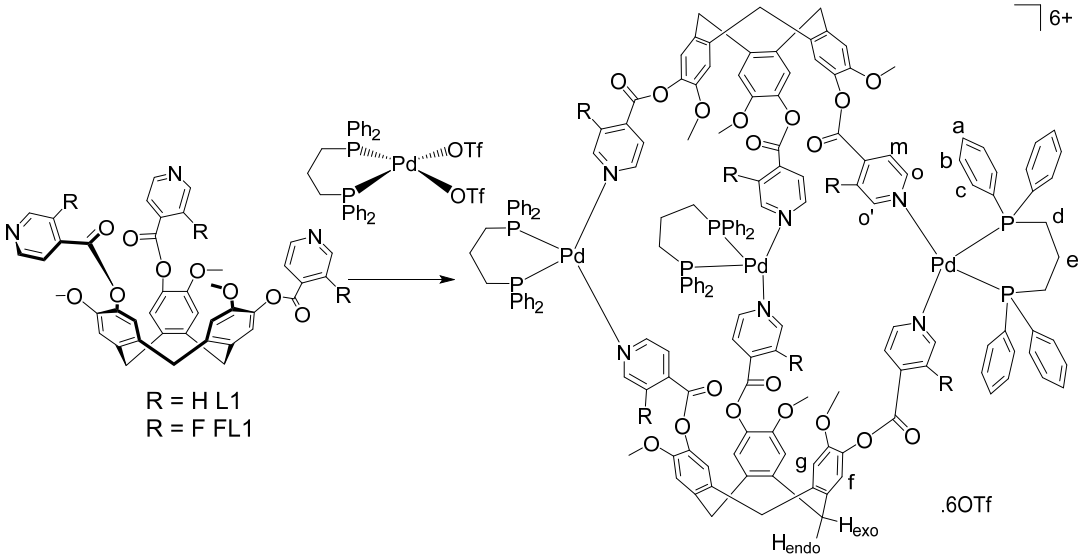

Scheme 2: Self-assembly of $[Pd_3(dppp)_3(L1)_2]^{6+}$ and $[Pd_3(dppp)_3(FL1)_2]^{6+}$ cages and numbering scheme for NMR assignments.

The ^{1}H NMR spectrum of a 3:2 mixture of $[Pd(dppp)(OTf)_2]$ and L1 in d_3-MeCN is well-resolved, with slight broadening consistent with complex formation. The spectrum retains high symmetry typical of a symmetric cage-species such as $[Pd_3(dppp)_3(L1)_2]^{6+}$. The ^{1}H Hm peak of L1 was shifted upfield by 0.21 ppm, and the Ha/Hb peaks of dppp, which are overlapping in the $[Pd(dppp)(OTf)_2]$ starting material, are resolved in the complex which is consistent with spectra of previously reported $[Pd_3(dppp)_3L_2]^{6+}$

metallo-cryptophanes.[5,6] The propylene Hd peak of the dppp was shifted downfield by 0.26 ppm. The ^{31}P NMR spectrum gave a single peak at ca. 8 ppm. The 2D ROESY ^{1}H NMR spectrum also gave evidence for metallo-crytophane formation with through-space connections observed between Ho protons of L1 and Hc and Hb of the dppp, Figure 5. Whether *syn*- or *anti*-$[Pd_3(dppp)_3L_2]^{6+}$ crytophanes are formed can be ascertained by behaviour of the He protons. In a D_3-symmetric *anti*isomer cryptophane a triplet is expected as He protons are homotopic, however they are diastereomeric in the *syn*-isomer and two peaks are expected[6] in a manner analogous to the NMR signals observed for $-(CH_2)_n-$ bridges of E (*anti*) and F (*syn*) cryptophanes.[23] Here, the He signal remains a broadened triplet on complexation indicative of the *anti*-isomer. Concentration effects on metallo-cage formation were probed with ^{1}H and ^{31}P NMR spectra recorded at concentrations between 0.5 mmol and 5.0 mmol. As the concentration increases, small amounts of the *syn*-isomer can be observed in solution. ^{31}P NMR spectra showed a second broad signal at ca. 10.5 ppm (SI Fig. S14), and close inspection of the ^{1}H NMR spectrum showed additional sets of broad peaks attributable to the *syn*-isomer (Figures 4 and S15). The 5.0 mM solution showed no changes with temperature and was stable to 65 °C.

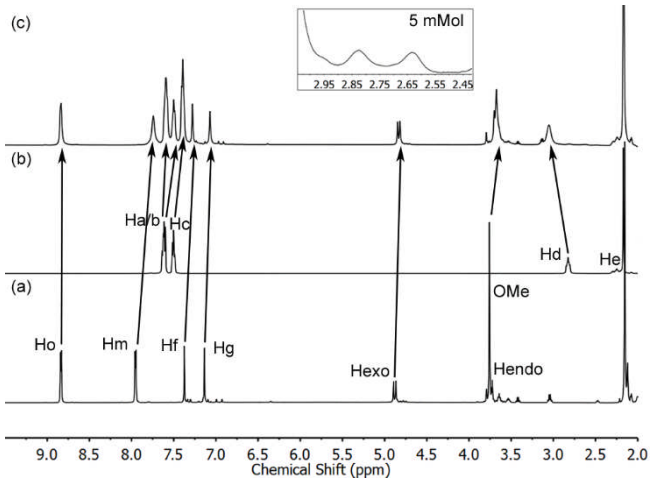

Figure 4. ^{1}H NMR (293 K, 500 MHz, d_3-MeCN) spectra of (a) L1; (b) [Pd(dppp)(OTf)$_2$]; (c) 3:2 mixture of L1 and [Pd(dppp)(OTf)$_2$] forming [Pd$_3$(dppp)$_3$(L1)$_2$]$^{6+}$ metallo-cryptophane as predominant anti-isomer, with inset showing diastereotopic He of syn-isomer observed at 5 mM concentration.

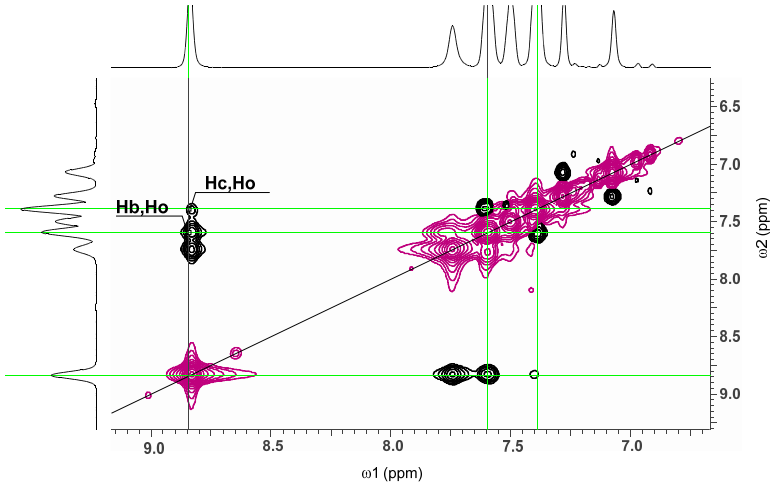

Figure 5. Section of the ^{1}H NMR (293 K, 500 MHz, d_3-MeCN) ROESY spectrum of [Pd$_3$(dppp)$_3$(L1)$_2$]·6(OTf). Exchange peaks are in grey and rOes in black with through-space connections between L1 and dppp marked.

The [Pd$_3$(dppp)$_3$(L1)$_2$]$^{6+}$ metallo-cryptophane also assembles in d_3-MeNO$_2$, with both *syn*- and *anti*-isomers present in 1:10 proportions at all concentrations studied. The presence of the *syn*- isomer was apparent from ^{1}H NMR spectroscopy, with the

diastereomeric He signals of the *syn-* isomer visible (Figure S16). The 2D ROESY spectrum in d_3-$MeNO_2$ was complicated by overlapping peaks, however, through-space connections between the L1 Ho and Hb of the dppp could be assigned, again consistent with cage formation (Figure S17).

Assembly of a $[Pd_3(dppp)_3(FL1)_2]^{6+}$ metallo-cryptophane with the fluorinated ligand FL1 also occurs in d_3-$MeNO_2$ solution. A 3:2 mixture of $[Pd(dppp)(OTf)_2]$ and FL1 in d_3-$MeNO_2$ gave a well resolved ^1H NMR spectrum, where the FL1 pyridyl Ho and Ho' are broadened and shifted downfield, and the Hd proton of the dppp undergoes a significant downfield shift of 0.42 ppm, Figure 6. 2D ROESY NMR analysis indicates through-space connections between Hb of the dppp and Ho and Ho' of the FL1 pyridyl groups, Fig. S19. It was noted that the resonance for the Hb protons of dppp appeared to be split into two resonances in the region of 7.7 ppm. This was confirmed by 2-D HMQC analysis (Fig. S20). ^{31}P NMR spectroscopy indicates a single phosphorous environment (Fig. S21). This, in addition to the broadened and individual peak for He dppp proton, indicates that the cage has formed stereoselectively as the *anti*-isomer. In this case, increasing concentration of the components in solution up to a maximum of 5.0 mMdid not lead to any changes in the NMR spectra. The $^{19}F\{^1H\}$ NMR spectrum revealed at least 5 different fluorine environments, with the most intense and sharpest at -120.2 ppm, indicating that in solution the C-F groups are in different orientations within the cryptophane, Fig. S22.

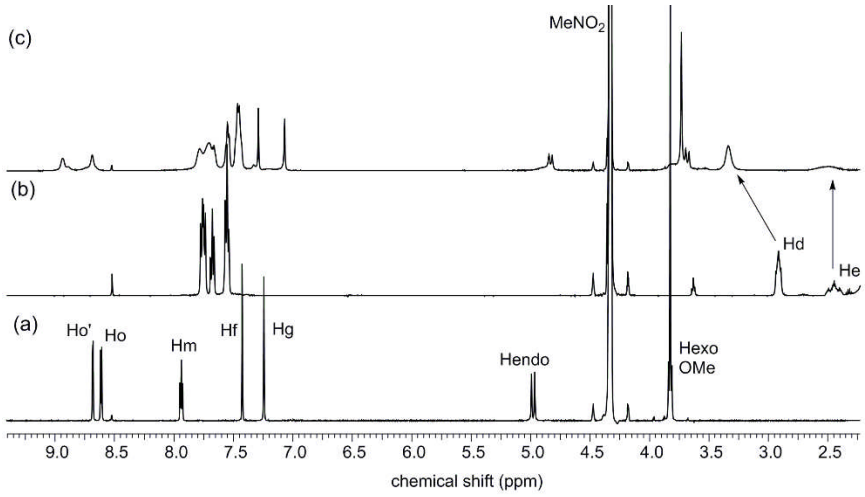

Figure 6. ^{1}H NMR (293 K, 500 MHz, d_3-$MeNO_2$) spectra of (a) FL1; (b) [Pd(dppp)(OTf)$_2$]; (c) 3:2 mixture of FL1 and [Pd(dppp)(OTf)$_2$] forming [Pd$_3$(dppp)$_3$(FL1)$_2$]$^{6+}$ metallo-cryptophane as the anti-isomer.

Combining [Pd(dppp)(OTf)$_2$] and FL1 in d_3-MeCN, however, resulted in a ^{1}H NMR spectrum that closely resembles a superposition of the spectra of the reactants, Figure S24. Furthermore, the 2D ROESY spectrum showed no through-space connections between the FL1 and the dppp ligand. Despite NMR studies not giving compelling evidence of the cage formation in d_3-MeCN solution, single crystals of the metallo-cryptophane [Pd$_3$(dppp)$_3$(FL1)$_2$]·6OTf were obtained from vapour diffusion of Et_2O into a MeCN solution of [Pd(dppp)(OTf)$_2$] and FL1 in 3:2 proportions. Their structure was determined by X-ray diffraction. Interestingly, the marked preference for an *anti*-[Pd$_3$(dppp)$_3$(L)$_2$]$^{6+}$ isomer observed in solution was not reflected in the crystal structure where the achiral *syn*-isomer is observed. It should be noted that the product of a crystallisation is not necessarily under thermodynamic control and depends on nucleation kinetics, with the first product to nucleate templating further crystal growth. A mass spectrum of the [Pd$_3$(dppp)$_3$(FL1)$_2$]·6OTf crystals re-dissolved in CH_3CN showed only a trace peak that was attributable to the cage (Fig. S31).

The structure of $[Pd_3(dppp)_3(FL1)_2]\cdot 6OTf$ was solved in the triclinic space group *P*-1 with a complete metallo-cryptophane and counter-anions in the asymmetric unit. As expected, the Pd(II) centres have approximate square planar geometry with a chelating dppp ligand (Pd-P bond lengths 2.249(3) to 2.286(3) Å) and coordinating pyridyl groups from two FL1 ligands of opposite chirality at Pd-N distances ranging from 2.110(8) to 2.160(8) Å. Each FL1 ligand binds to three Pd(II) centres to form the cage-like assembly. The cage has a trigonal bipyramidal shape with the Pd(II) cations forming an equatorial plane with Pd···Pd separations ca. 18 Å. Rotation of the six fluoro-isonicotinoyl groups of the assembly are all slightly different, with the majority having the carbonyl group *exo* to the cage cavity and only one with and *endo* carbonyl. There is no rotational disorder apparent and positions of the fluorine atoms are well resolved in an approximately C_3-symmetry relationship per FL1 ligand, and with C-F groups of different FL1 ligands aligning in an eclipsed manner when the cage is viewed axially.

There are face-to-face π-π stacking interactions between the pyridyl groups of FL1 and phenyl groups of the dppp, with ring centroid separations 3.43-3.72 Å. These close interactions are consistent with the through space connections observed by ROESY NMR in d_3-$MeNO_2$. The triflate counter-anions form second sphere electrostatic interactions with the Pd(II) centres at S-O···Pd distances ca. 2.9-4.2 Å. Not all triflate positions could be refined within the structure but electron density difference maps indicate the excluded anions are also in similar positions around Pd(II) centres. As for other metallo-cryptophanes there is no evidence of counter-anion encapsulation inside the cage.[6]

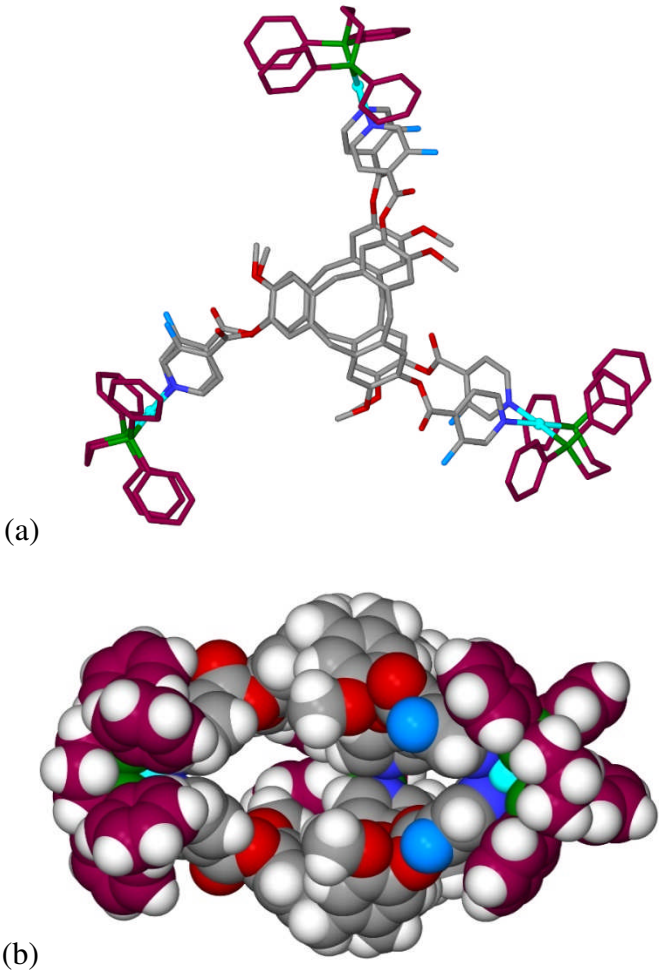

Figure 7. From the X-ray structure of [Pd$_3$(dppp)$_3$(FL1)$_2$]·6OTf. (a) syn-[Pd$_3$(dppp)$_3$(FL1)$_2$]$^{6+}$ cage viewed down axial direction; (b) space-filling view of cage from side. Dppp ligands shown in purple.

Trans-linked M_3L_2 cages with L2

A 3:2 mixture of *trans*-[PdCl$_2$(MeCN)$_2$] and L2 were reacted in deuterated dimethylformamide (d$_7$-DMF) or dimethylsulfoxide (d$_6$-DMSO) with the aim of forming the trans-linked metallo-cryptophane, according to Scheme 3. The ^{1}H NMR spectra of the resultant solutions were very broad, though a sharp signal was observed for uncomplexed MeCN which indicates that these have been displaced from the *trans*-[PdCl$_2$(MeCN)$_2$] by the imidazolyl-moieties of L2 (SI Figs. S27, S28). However, the severe broadening and number of signals for the L2 peaks is not indicative of a single,

symmetric product. The high resolution electrospray mass spectrum from either solvent is dominated by a singly charged peak at *m/z* 941.1833 for species $\{PdCl(L2)\}^+$. However, a small peak was also observed at *m/z* 2134.2070 which corresponds to the expected isotope pattern for $\{Pd_3Cl_5(L2)_2(MeCN)\}^+$, the desired metallo-cryptophane with the loss of one Cl^-, Figure 8 and Fig. S32.

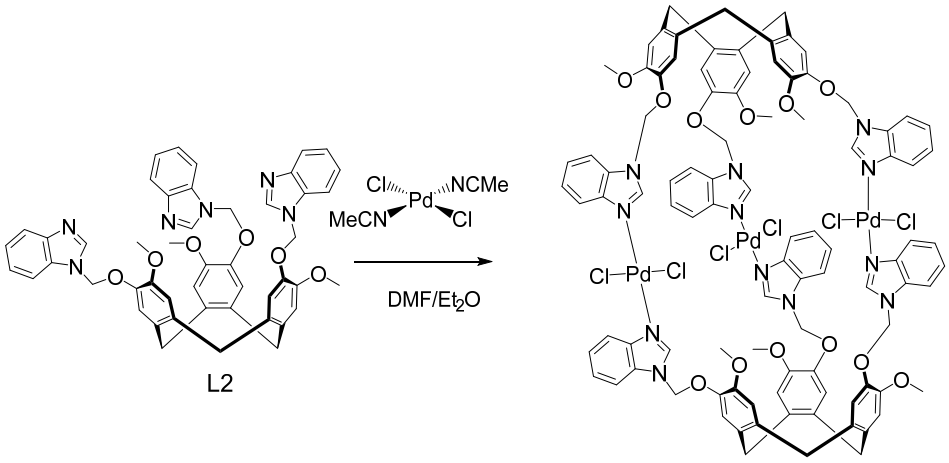

Scheme 3: Assembly of trans-linked cage anti-$[Pd_3Cl_6(L2)_3]$ observed by mass spectrometry and in the solid state.

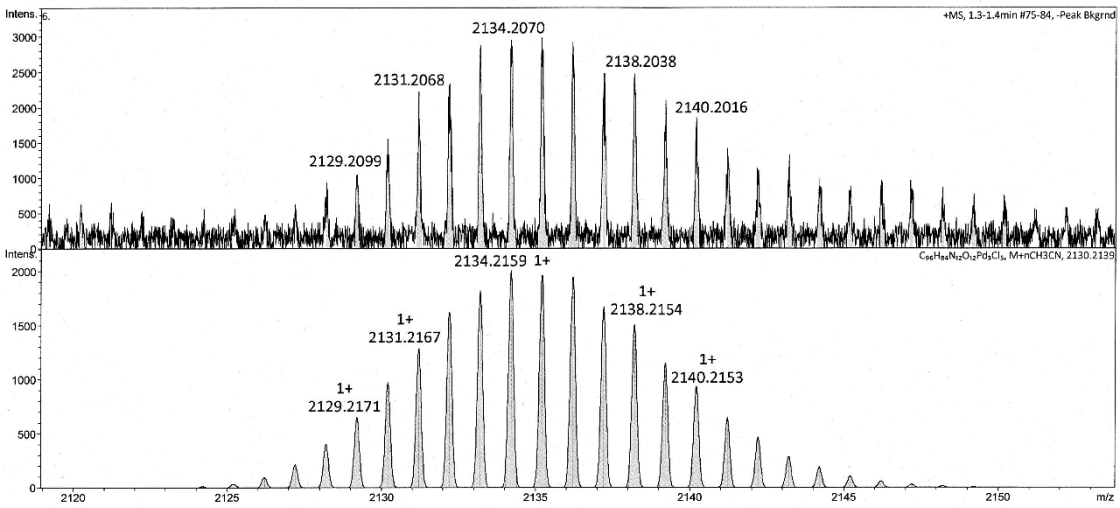

Figure 8: Detail from ESI-MS of $[Pd_3Cl_5(L2)_3]^+$ observed (top) and calculated (bottom).

Single crystals of composition $[Pd_3Cl_6(L2)_3\cdot(H_2O)]\cdot 1.5H_2O\cdot 3DMF$ are formed from a DMF solution containing *trans*-$[PdCl_2(MeCN)_2]$ and L2 in 3:2 proportions that was stirred for 24 hours then subjected to diffusion of diethyl ether vapours. Initially a yellow powder forms and single crystals form after 3 months. Powder and crystals are insoluble once precipitated, and powder XRD indicates the powder is amorphous. The complex crystallises with a cubic unit cell and the structure was solved in space group *Pa*-3 and shows the anticipated $[Pd_3Cl_6(L2)_3]$ metallo-cryptophane cage. The structure has crystallographic 3-fold symmetry with one third of the assembly in the asymmetric unit, alongside an additional molecule of DMF, a partially occupied H_2O *exo* to the cage and a disordered water inside the cage.

The Pd(II) centre features *trans* coordination of terminal Cl^- ligands at Pd-Cl distances 2.2747(15) and 2.2944(15) Å, and two *trans* benzimidazole groups at Pd-N distances 2.012(4) and 2.013(5) Å. The two benzimidazole groups belong to crystallographically distinct L2 ligands and are not coplanar with respect to the coordinated Pd(II) with torsion angle between the planes ca. 53°. The L2 ligand coordinates to three symmetry equivalent Pd(II) centres to form a cage-like metallo-cryptophane assembly, Figure 9. Within a cage assembly, both L2 ligands are of the same chirality thus the *anti*-isomer is formed. Overall the structure is racemic. For both types of L2 ligand, the orientation of the benzimidazole groups with respect to the CTG-scaffolds are similar, with the benzene moieties *exo* to the cavitand bowl but the imidazole CH groups pointing in towards the CTG cavity. C_{arene}-O-CH_2-N_{imid} torsion angles are 66.3 and 73.4°, and benzimidazole groups of different L2 ligands within the cage are near co-planar. There are face-to-faceπ-π stacking interactions between the imidazole groups with centroid separation 3.465 Å. The equatorial M_3 trigonal plane is pinched in towards the inside of the capsule structure, with Pd···Pd separations 5.735 Å.

This compares with Pd···Pd distances of 17.7-18 Å for $[Pd_3(dppp)_3(L1)_2]^{6+}$. This limits window size and the space available for guest binding within the cage, as can be seen in the space filling diagram Figure 9b. A molecule of water that was disordered across the 3-fold axis was observed as an intra-cage guest with closest contacts to the imidazole C-H groups at C···O separation 2.57 Å. Cages of alternating chirality pack in a checkerboard fashion in the crystal lattice, Figure 9c.

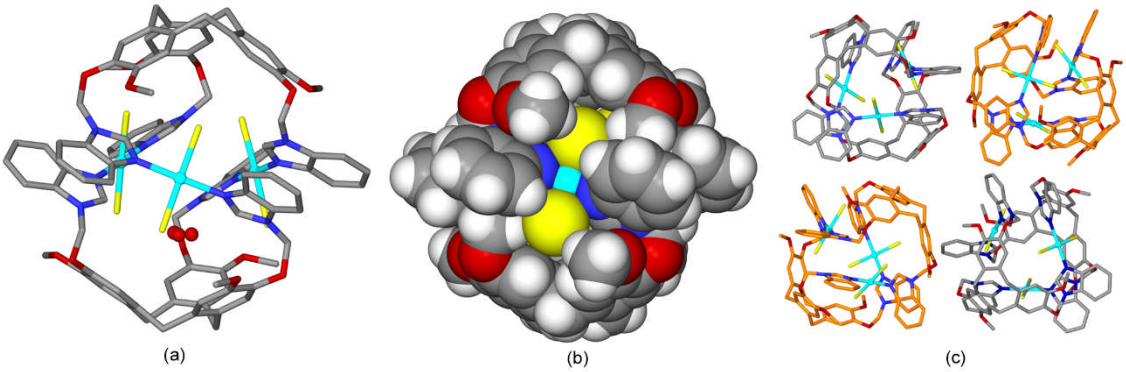

Figure 9. From the X-ray structure of $[Pd_3Cl_6(L2)_2\cdot(H_2O)]\cdot 1.5H_2O\cdot 3DMF$. (a) $[Pd_3Cl_6(L2)_2]$ metallocryptophane with disordered water guest, hydrogen atoms omitted for clarity; (b) space filling representation of $[Pd_3Cl_6(L2)_2]$; (c)checkerboard arrangement of different enantiomers of the cage.

Experimental

Synthesis

(±)-Cyclotriguaiacylene,[24] *tris*(iso-nicotinoyl)cyclotriguaiacylene (L1),[16b] and 1-(chloromethyl)benzimidazole hydrochloride [25] were synthesised by literature methods. All other chemicals were obtained from commercial sources and were used without further purification. NMR spectra were recorded by automated procedures on a Bruker

Avance 300 MHz, 500 MHz NMR or Varian Unity Inova 500 spectrometer. Electrospray mass spectra (ES-MS) were measured on a Bruker Maxis Impact instrument in positive ion mode. Infra-red spectra were recorded as solid phase samples on a Bruker ALPHA Platinum ATR. Elemental analyses were performed on material that had been washed with diethyl ether, subsequently dried at 80-90 ˚C under vacuum and then exposed to the atmosphere.

(±)-2,7,12-Trimethoxy-3,8,13-*tris*(3-fluoro-4-pyridylcarboxy)-10,15-dihydro-5*H*-tribenzo[a,d,g]cyclononene (FL1). *Part 1:* 3-Fluoro-4-pyridine carboxylic acid (2.01 g, 12.858 mmol) was suspended in thionyl chloride (12 mL, excess) and heated at reflux for three hours, during which time it turned from colourless to orange. Excess thionyl chloride was removed *in vacuo* to yield 3-fluoro-4-pyridine carbonyl chloride hydrochloride (980 mg, 4.655 mmol) in quantitative yield which was used without further purification. *Part 2:* Anhydrous triethylamine (2.71 mL, 12.40 mmol) was added to a stirred solution of CTG (645 mg, 1.58 mmol) in anhydrous tetrahydrofuran (240 mL) at -78 °C, under an argon atmosphere. After one hour, 3-fluoro-4-pyridine carbonyl chloride hydrochloride (980 mg, 4.65 mmol) was added to the reaction mixture and stirred at -78 °C for a further two hours, before being left to stir at room temperature for 48 hours. A second portion of 3-fluoro-4-pyridine carbonyl chloride hydrochloride (980 mg, 4.65 mmol) was added and left to stir for a further 48 hours, during which time the reaction mixture discoloured. All volatiles were removed *in vacuo*, and the resultant residue triturated in ethanol to afford the target compound as a white solid. Yield 1062 mg, 89 %; m.p. decomposes > 270 °C; HRMS (ES^+): *m/z* 778.2228 $\{MH\}^+$; calculated for $C_{42}H_{31}F_3N_3O_9$ 778.2012; ^1H NMR (300 MHz, d_6-DMSO) δ (ppm) = 8.87 (d, 3H, Ho', J = 2.3 Hz), 8.69 (d, 3H, Ho, J = 4.9 Hz), 7.97 (dd, 3H, Hm, J = 6.0, 5.1 Hz), 7.58

(s, 3H, Hf), 7.34 (s, 3H, Hg), 4.90 (d, 3H, H_{exo}, J = 13.5 Hz), 3.74 (s, 9H, O-CH_3), 3.71 (d, 3H, H_{endo}, J = 13.5 Hz); $^{19}F\{^1H\}$ NMR (300 MHz, d_6-DMSO) δ (ppm) = - 125.63; $^{13}C\{^1H\}$ NMR (75 MHz, d_6-DMSO) δ (ppm) = 160.3, 158.2, 154.6, 149.0, 146.8, 140.7, 139.1, 137.2, 131.9, 124.4, 123.9, 114.6, 56.3, 34.6; Analysis for $C_{42}H_{30}F_3N_3O_9 \cdot 0.5(H_2O)$ (% calculated, found) C (64.12, 64.30), H (3.97, 3.85), N (5.34, 5.30); FT-IR (cm^{-1}) 3017, 2976, 2920, 1737, 1607, 1564, 1506, 1442, 1324, 1263, 1205.

(±)-2,7,12-Trimethoxy-3,8,13-*tris*(methylbenzimidazol-1-yl)-10,15-dihydro-5*H*-tribenzo[a,d,g]cyclononene (L2) CTG (400 mg, 0.98 mmol) was added to a suspension of NaH (60% dispersion in mineral oil) (0.84 g, 20.8 mmol) in anhydrous, degassed DMF (10 mL) under a nitrogen atmosphere at room temperature, and stirred for 30 mins. 1-(chloromethyl)benzimidazole hydrochloride (694 mg, 3.4 mmol) was added in portions and the mixture stirred for 16 h. Water (100 mL) was added and the resulting grey precipitate filtered. The grey residue was re-dissolved in dichloromethane (60 mL), dried over $MgSO_4$, and solvents removed *in vacuo*. The residue was sonicated in diethyl ether (50 mL), affording the title compound as a white solid. Yield 0.58 g, 0.73 mmol, 75%; HRMS (ESI^+) 821.3065 $\{MNa\}^+$, calculated for $\{C_{48}H_{42}N_6NaO_6\}^+$ 821.3059; ^1H NMR (300 MHz, DMSO-d_6) δ (ppm) 8.35 (s, 3H, H^1), 7.65 (dd, 3H, J = 6.1, 2.9 Hz, H^6) , 7.59-7.55 (m, 3H, H^3), 7.25-7.20 (m, 6H, H^4, H^5), 7.18 (s, 3H, H^{10}), 7.04 (s, 3H, H^{11}), 6.20-6.10 (m, 6H, H^8), 4.69 (d, 3H, J = 13.5 Hz, *endo*-H^{16}), 3.67 (s, 9H, H^9), 3.47 (d, 3H, J = 13.6 Hz, *exo*-H^{16}); $^{13}C\{^1H\}$ NMR (75 MHz, DMSO-d_6) δ (ppm) 148.76 (C^{13}), 144.34 (C^1), 143.50 (C^2), 143.46 (C^7), 134.88 (C^{15}), 133.47 (C^{12}), 131.79 (C^{14}), 122.90 (C^5), 122.21 (C^4), 119.51 (C^6), 119.01 (C^{10}), 114.34 (C^{11}), 110.76 (C^3), 73.03 (C^8), 55.93 (C^9), 35.06 (C^{16}); Elemental analysis for $C_{48}H_{42}N_6O_6 \cdot 1.5(H_2O)$ Calcd. C 69.79, H 5.50, N 10.18; Found: C 69.82, H 5.01, N 10.32; FT-IR (cm^{-1}) 3092, 2958, 2926, 1611, 1452, 1273, 1198, 970, 745.

$[Pd_3(dppp)_3(L)_2]\cdot 6OTf$ cage assembly

General procedure for NMR experiments: 3:2 stoichiometric mixtures of $[Pd(dppp)(OTf)_2]$ and L-ligand at approximately 5 mM concentration (unless otherwise specified) were prepared from stock solutions in the appropriate deuterated solvent, and mixed using a vortex. ^{1}H NMR assignments for representative solution are given below, details of further experiments are in supplementary information.

$[Pd_3(dppp)_3(L1)_2]\cdot 6OTf$ ^{1}H NMR (500 MHz, d_3-MeCN) δ (ppm) δ 8.83 (s, 5H, Ho), 7.74 (s, 6H, Hm), 7.60 (s, 12H, Hb), 7.50 (7H, s, Ha), 7.39 (s, 12H, Hc), 7.28 (s, 3H, Hf), 7.07 (s, 3H, Hg), 4.83 (d, 3H, *J* = 13.7 Hz, Hexo), 3.69 (d, 12H, *J* = 13.5 Hz, Hendo+OMe), 3.05 (s, 5H, Hd), 2.24 (s, overlapping with solvent, He).

$[Pd_3(dppp)_3(FL1)_2]\cdot 6OTf$ ^{1}H NMR (500 MHz, d_3-$MeNO_2$) δ (ppm) 8.94 s, 3H, Ho/o'), 8.69 (s, 3H, Ho/o'), 7.79-7.66 (m, 18H, Hm+Hb), 7.55 (s, 8H, Ha), 7.52-7.38 (m, 15H, Hc), 7.29 (s, 3H, Hf), 7.07 (s, 3H, Hg), 4.83 (d, 3H, *J* = 13.7 Hz, Hendo), 3.73 (s, 9H, OMe), 3.68 (d, 3H, *J* = 13.9 Hz, Hexo), 3.34 (s, 7H, Hd), 2.49 (s, 3H, He)

Single crystals of $[Pd_3(dppp)_3(FL1)_2]\cdot 6OTf$ were grown by vapour diffusion of diethyl ether into a solution of components in acetonitrile. Elemental analysis for $[Pd_3(dppp)_3(FL1)_2]\cdot 6OTf$ Calcd.: C 51.26, H 3.47, N 2.10; Found: C 50.99, H 3.38 N 2.10; HRMS (ESI$^+$) *m/z* 1853.3262 for $\{[Pd_3(dppp)_3(FL1)_2]\cdot 4OTf\}^{2+}$ (minor peak); FT-IR (cm^{-1}) 1750, 1509, 1436, 1313, 1271, 1244, 1224, 1159, 1097, 1066, 1027, 999, 974, 837, 745, 707, 691, 672, 637, 573, 513.

$[Pd_3Cl_6(L2)_2]$ metallo-cryptophane A solution of L2 (7 mg, 8 μmol) and $[PdCl_2(MeCN)_2]$ (3.4 mg, 13 μmol) in DMF (1 mL) was stirred for 24 h. Two drops were taken for HRMS characterisation, and the rest set up as a vapour diffusion with diethyl ether anti-solvent. A pale yellow solid precipitated after one week, and small

number of pale yellow blocks grew after three months. HRMS (ESI$^+$) *m/z* 941.1833 for species {PdCl(L2)}$^+$, 2134.21 {$Pd_6Cl_5L_2(MeCN)$}$^+$; FT-IR (cm^{-1}) 1611, 1508, 1264, 1182, 1141, 1066, 1025, 742**.** Satisfactory microanalysis was not obtained from powdered material which is likely a mixture of cage and $PdCl_2$: Found C 47.39 H 3.41 N 7.73 % Calcd. for [$Pd_3Cl_6(L2)_2$] C 54.12, H 3.98, N 7.89; for [$Pd_3Cl_6(L2)_2$].$PdCl_2$ C 49.96, H 3.67, N 7.29.

X-Ray Crystallography

Crystals were mounted under inert oil on a MiTeGen tip and flash frozen to 150(1) K. X-ray diffraction data were collected using Cu-$K\alpha$ radiation (λ= 1.54184 Å) using an Agilent Supernova dual-source diffractometer with Atlas S2 CCD detector and fine-focus sealed tube generator, or using synchrotron radiation (λ= 0.6889 Å) at station I19 of Diamond Light Source (co-crystal (L2)·(CTG)). Data were corrected for Lorenztian and polarization effects and absorption corrections were applied using multi-scan methods. The structures were solved by direct methods using SHELXS-97 and refined by full- or block-matrix on F^2 using SHELXL-97.[26] Unless otherwise specified, all non-hydrogen atoms were refined as anisotropic, and hydrogen positions were included at geometrically estimated positions. Additional details of data collections and structure solutions are given below and in Table 1.

(L2)·(CTG) Crystals were of poor quality with poor internal consistency (R_{int} = 0.1652) and did not diffract to high angles even with the use of synchrotron radiation.

[Pd_3(dppp)$_3$(FL1)$_2$]·6OTf The Pd, coordinating P atoms and non-hydrogen atoms of the FL1 ligand were refined as anisotropic, with all other atoms refined with an isotropic model. Crystals did not diffract at high angles and attempts to grow higher quality crystals were not successful. Only four of the six triflate counter-anions could be

located in the difference map and refined, so two have been excluded from refinement but are included in the formula. One aromatic ring was refined with a rigid body constraint, some interatomic distances were restrained to be chemically reasonable, and restraints were placed on some anisotropic displacement parameters. The structure contained significant void space (ca. 35% of unit cell volume) with residual electron density which could not be meaningfully modelled as solvent nor counter-anions, hence the SQUEEZE routine of PLATON was employed.[27]

$[Pd_3Cl_6(L2)_3\cdot(H_2O)]\cdot 1.5H_2O\cdot 3DMF$ One guest water showed symmetry disorder across three positions, and another was refined at 0.5 occupancy. Hydrogen positions were not included for water molecules. Water and DMF solvent were refined isotropically.

Table 1: Details of X-ray data collections and structure refinements.

Compound	L2	(L2)·(CTG)	$[Pd_3(dppp)_3(FL1)_2]$ ·6OTf	$[Pd_3Cl_6(L2)_3\cdot(H_2O)]$ ·1.5H_2O·3DMF
CCDC	1552584	1552583	1552585	1552586
Formula	$C_{48}H_{42}N_6O_6$	$C_{72}H_{66}N_6O_{12}$	$C_{171}H_{135}F_{24}N_6O_{36}P_6Pd_3S_6$	$C_{105}H_{110}Cl_6N_{15}O_{17.5}Pd_3$
Mr	798.88	1207.31	1029.21	2393.98
Crystal size	0.31 x 0.05 x 0.05	0.05 x 0.02 x 0.02	0.07 x 0.05 x 0.01	0.07 x 0.06 x 0.05
Crystal system	Triclinic	Trigonal	Triclinic	Cubic
Space group	*P*-1	*Pc*31	*P*-1	*Pa*-3
a (Å)	10.7347(5)	19.4199(10)	18.8882(4)	27.7884(3)
b (Å)	12.6277(4)	19.4119(10)	22.7914(4)	27.7884(3)
c (Å)	14.8026(6)	9.0953(8)	28.1888(6)	27.7884(3)
α (^{0})	83.722(3)	90	102.532(2)	90
β (^{0})	86.985(4)	90	10.5.751(2)	90
γ (^{0})	79.149(3)	120	93.501(2)	90
V (Å^3)	1957.81(14)	2968.1(3)	11307.7(4)	21458.1(4)
Z	2	2	2	8
ρ_{calc} (g.cm^{-3})	1.355	1.351	1.176	1.482
θ range (^{0})	3.58-73.75	2.03-20.14	3.29-65.0	3.18-73.79
No. data collected	15677	23054	89198	19190
No. unique data	7391	2079	37073	7084
R_{int}	0.0281	0.1652	0.1095	0.0430

No. obs. Data ($I > 2\sigma(I)$)	6235	1967	17537	5598
No. parameters	544	273	1516	414
No. restraints	0	1	9	0
R_1 (obs data)	0.0375	0.0766	0.1051	0.0675
wR_2 (all data)	0.0927	0.1951	0.3059	0.1994
S	1.022	1.114	0.955	1.040

Conclusions

Metal-organic cryptophanes with capsule-like structures were successfully synthesised using iso-nicotinoyl-appended CTG-ligands and Pd(dppp) as the metal-fragment. The *anti*-isomers are the dominant species in solution, and solution assembly was found to be solvent dependent with $[Pd_3(dppp)_3(L1)_2]\cdot 6(OTf)$ observed in both CD_3CN and CD_3NO_2 whilst $[Pd_3(dppp)_3(L1)_2]\cdot 6(OTf)$ was only seen in CD_3NO_2. Nevertheless, crystals of *syn*-$[Pd_3(dppp)_3(L1)_2]\cdot 6(OTf)$ grew from CD_3CN solution. The inability to form stable $[Pd_3(en)_3(L)_2]^{6+}$ capsules, where the protecting chelating ligand is ethylenediamine, is in keeping with our previous report.[7] Cryptophane structures can also be accessed from metal fragments that have *trans* available coordination sites, exemplified by the neutrally charged complex $[Pd_3Cl_6(L2)_3]$ whose crystal structure revealed formation as the *anti*-isomer. Here the internal space within the capsule is limited by the encapsulation of the *trans*-$PdCl_2$ fragment inside the capsule, however a water guest was observed inside the cage by crystallography.

Acknowledgements

We thank the EPSRC for funding (EP/J001325/1, EP/K039202/1, DTG studentship awards to JMF and JJH). We thank Stephen Boyer and Tanya Marinko-Covell for

microanalysis. This work was carried out with support of Diamond Light Source (MT-10334).

Data accessibility

Data supporting this study can be accessed at http://####################.

References

(1) for reviews see (a) Hardie, M. J. in *Supramolecular Chemistry: From Molecules to Nanomaterials*, John Wiley and Sons, Eds. Gale, P. A.; Steed, J. W. **2012**, *3*, 895-916; (b) Brotin, T.; Dutasta, J.-P. *Chem. Rev.* **2009**, *109*, 88-130; (c) Collet, A.; Dutasta, J.-P.; Lozach, B. *Adv. Supramol. Chem.* **1993**, *3*, 1-35; (d) Collet, A. *Tetrahedron* **1987**, *43*, 5725-5759.

(2) reviews (a) Wang, Y.; Dmochowski *Acc. Chem. Res.* **2016**, *49*, 2179-2187; (b) Palaniappan, K. K.; Francis, M. B.; Pines, A.; Wemmer, D. E. *Isr. J. Chem.* **2014**, *54*, 104-112.

(3) for example Chaffee, K. E.; Fogarty, H. A.; Brotin, T.; Goodson, B. M.; Dutasta, J.-P. *J. Phys. Chem. A* **2009**, *113*, 13675-13684.

(4) reviews (a) Hardie, M. J. *Chem. Lett.* **2016**, 45, 1336-1346; (b) Henkelis, J. J.; Hardie, M. J. *Chem. Commun.* **2015**, *51*, 11929-11943.

(5) Zhong, Z.; Ikeda, A.; Shinkai, S.; Sakamoto, S.; Yamaguchi, K. *Org. Lett.* **2001**, *3*, 1085–1087.

(6) Schaly, A.; Rousselin, Y.; Chambron, J.-C.; Aubert, E.; Espinosa, E. *Eur. J. Inorg. Chem.* **2016**, 832–843.

(7) Henkelis, J. J.; Carruthers, C. J.; Chambers, S. E.; Clowes, R.; Cooper, A. I.; Fisher, J.; Hardie, M. J. *J. Am. Chem. Soc.* **2014**, *136,* 14393–14396.

(8) Pritchard, V. E.; Rota Martir, D.; Oldknow, S.; Kai, S.; Hiraoka, S.; Cookson, N. J.; Zysman-Colman, E.; Hardie, M. J. *Chem. Eur. J.* **2017**, 23, 6290-6294.

(9) Henkelis, J. J.; Ronson, T. K.; Harding L. P.; Hardie, M. J. *Chem. Commun.*, **2011**, *47*, 6560-6562.

(10) Westcott, A.; Fisher, J.; Harding, L. P.; Rizkallah, P.; Hardie, M. J. *J. Am. Chem. Soc.* **2008**, *130*, 2950-2951.

(11) (a) Wie, J.; Li, Z.-M.; Jin, X.-J.; Yao, X.-J.; Cao, X.-P.; Chow, H.-F.; Kuck, D. *Chem. As. J.* **2015**, *10*, 1150-1158; (b) Ronson, T. K.; Nowell, H.; Westcott, A.; Hardie, M. J. *Chem. Commun.* **2011**, *47*, 176-178.

(12) for example (a) Yamanaka, M.; Yamada, Y.; Sei, Y.; Yamaguchi, K.; Kobayashi, K. *J. Am. Chem. Soc.* **2006**, *128*, 1531-1539; (b) Pirondini, L.; Bonifazi, D.; Cantadori, B.; Braiuca, P.; Campagnolo, M.; Zorzi, R. D.; Geremia, S.; Diederich, F.; Dalcanale, E. *Tetrahedron* **2006**, *62*, 2008–2015; (c) Zuccaccia, D.; Pirondini, L.; Dalcanale, E.; Macchioni, A. *J. Am. Chem. Soc.* **2005**, *127*, 7025-7032; (d) Cotton, F. A.; Lei, P.; Lin, C.; Murilo, C. A.; Wang, X.; Yu, S.-Y.; Zhang, Z.-X. *J. Am. Chem. Soc*. **2004**, *126*, 1518-1525; (e) Kobayashi, K.; Yamada, Y.; Yamanaka, M.; Sei, Y.; Yamaguchi, K. *J. Am. Chem. Soc.* **2004**, *126*, 13896–13897; (f) Jacopozzi, P.; Dalcanale, E. *Angew. Chem., Int. Ed. Engl.* **1997**, *36*, 613–615; (g) Park, S. J.; Hong, J.-I. *Chem. Commun.* **2001**, 1554–1555.

(13) Takenaka, K.; Obora, Y.; Jiang, L. H.; Tsuji, Y. *Organometallics* **2002,** *21*, 1158-1161.

(14) Haino, T.; Kobayashi, M.; Chikaraishi M.; Fukazawa, Y. *Chem. Commun.* **2005**, 2321–2323

(15) (a) Cookson, N. J.; Henkelis, J. J.; Ansell, R. J.; Fishwick, C. W. G.; Hardie, M. J.; Fisher, J. *Dalton Trans*. **2014**, *43*, 5657-5661; (b) Henkelis, J. J.; Fisher, J.; Warriner, S.

L.; Hardie, M. J. *Chem. Eur. J.* **2014**, *20*, 4117-4125; (c) Ronson, T. K.; Carruthers, C.; Fisher, J.; Brotin, T.; Harding, L. P.; Rizkallah, P. J.; Hardie, M. J. *Inorg. Chem.* **2010**, *49*, 675-685; (d) Ronson, T. K.; Fisher, J.; Harding L. P.; Hardie, M. J. *Angew. Chem. Int. Ed.* **2007**, *46*, 9086-9088.

(16) (a) Thorp-Greenwood, F. L.; Ronson, T. K.; Hardie, M. J. *Chem. Sci.* **2015**, *6*, 5779-5792; (b) Hardie, M. J.; Sumby, C. J. *Inorg. Chem.* **2004**, *43*, 6872-6874.

(14) Thorp-Greenwood, F. L.; Kulak, A. N.; Hardie, M. J. *Nature Chem.* **2015**, *7*, 526-531.

(17) (a) Payne, R. M.; Oliver, C. L. *CrystEngComm* **2016**, *18*, 7965; (b) Caira, M. R.; Jacobs, A.; Nassimbeni, L. R. *Supramol. Chem.* **2004**, *16*, 337-342; (c) Steed, J. W.; Zhang, H.; Atwood, J. L. *Supramol. Chem.* **1996***, 7*, 37-45; (d) Zhang H.; Atwood, J. L. *J. Crystallogr. Spectrosc. Res.* **1990**, 20, 465–470.

(18) (a) Rao, M. L. N.; Talode, J. B. *Asian J. Org. Chem.* **2016**, *5*, 98-106; (b) Thorp-Greenwood, F. L.; Pritchard, V. E.; Coogan, M. P.; Hardie, M. J. *Organometallics* **2016**, *35*, 1632-1642.

(19) (a) Fowler, J. M.; Thorp-Greenwood, F. L.; Warriner, S. L.; Willans, C. E.; Hardie, M. J. *Chem. Commun.* **2016**, *52*, 8699-8702; (b) Henkelis, J. J.; Barnett, S. A.; Harding, L. P.; Hardie, M. J. *Inorg. Chem.* **2012**, *51*, 10657-10674.

(20) for reviews see (a) Mukherjee, S.; Mukherjee, P. S. *Chem. Commun.* **2014**, *50*, 2239-2248; (b) Fujita, M.; Tominaga, M.; Hori, A.; Therrien, B. *Acc. Chem. Res.* **2005**, *38*, 369-378; (c) Fujita, M.; Umemoto, K.; Yoshizawa, M.; Fujita, N.; Kusukawa, T.; Biradha, K. *Chem. Commun.* **2001**, 509-518.

(21) Chand, D. K.; Manivannan, R.; Sahoo, H. S.; Jeyakumar, K. *Eur. J. Inorg. Chem.* **2005**, 3346-3352.

(22) Garcia, C.; Humilière, D.; Riva, N.; Collet, A.; Dutasta, J.-P. *Org. Biomol. Chem.* **2003**, *1,* 2207-2216.

(23) (a) Scott, J. L.; MacFarlane, D. R.; Raston, C. L.; Teoh, C. M. *Green Chem.* **2000**, *2*, 123-126; (b) Canceill, J.; Collet, A.; Gottarelli, G. *J. Am. Chem. Soc.* **1984**, *106*, 5997-6003.

(24) Schnopp, M.; Haberhauser, G. *Eur. J. Org. Chem.* **2009**, 4458-4467

(25) Sheldrick, G. M. *Acta Crystallogr. A* **2008**, *A64*, 112-122.

(26) Van der Sluis, P.; Spek, A. L. *Acta Crystallogr. A* **1990**, *A46*, 194-201.